# The Influence of Crystallographic Orientation on Crack Tip Displacements of Microstructurally Small, Kinked Crack Crossing the Grain Boundary

Igor Simonovski [a,*], Karl-Fredrik Nilsson [b], Leon Cizelj [a]

[a] *Jožef Stefan Institute, Reactor Engineering Division, Jamova 39, SI-1000 Ljubljana, Slovenia*

[b] *Institute for Energy, European Commission, DG-JRC, Postbus 2, 1755 ZG Petten, The Netherlands*

---

**Abstract**

The paper presents an analysis of the effects of grain orientations on a short, kinked surface crack in a 316L stainless steel. The kinking of the crack is assumed to take place at the boundary between two neighbouring grains. The analysis is based on a plane-strain finite element crystal plasticity model. The model consists of 212 randomly shaped, sized and oriented grains, loaded monotonically in uniaxial tension to a maximum load of $0.9R_{p0.2}$ (240 MPa). The influence that a random grain structure imposes on a Stage I crack is assessed by calculating the crack tip opening (CTOD) displacements for bicrystal as well as for polycrystal models, considering different crystallographic orientations. Since a Stage I crack is assumed, the crack is always placed in a slip plane. Results from a bicrystal case show that the maximal CTODs are directly related to the stiffness of the grain containing

the crack extension. Anisotropic elasticity and crystal plasticity both contribute to this grain stiffness, resulting in maximal CTOD when Schmid factors are the highest on two slip planes. Such crystallographic orientation results in a soft elasto-plastic response. Anisotropic elasticity can additionally increase the softness of a grain at certain crystallographic orientations. Minimal anisotropic elasticity at the crystallographic orientations with the highest Schmid factors causes the CTOD to be maximized. Presuming that the crack will preferably follow the slip plane where the crack tip opening displacement is highest, we show that the crystallographic orientation can affect the CTOD values by a factor of up to 7.7. For a given grain orientation the maximum CTOD is attained when the crack extension deflection into a second grain is between -75.141° and 34°. For the polycrystal case we show that grains beyond the first two crack-containing grains change the CTOD by a factor of up to 3.3 and that the largest CTODs are obtained when placing the crack into a slip plane with crack extension that results in a crack extension being more perpendicular to the external load.

*PACS:* 46.50.+a; 61.50.-f; 62.20.Mk

*Key words:* Small cracks; crack tip displacements; polycrystalline material; crystal plasticity; grain boundary.

---

* Corresponding author. Address: Jožef Stefan Institute, Reactor Engineering Division, Jamova 39, SI-1000 Ljubljana, Slovenia. Tel.: +386 1 5885 290. Fax.: +386 1 5885 377

*Email address:* igor.simonovski@ijs.si (Igor Simonovski).

*URL:* http://www.rcp.ijs.si/isimonovski/ (Igor Simonovski).

## 1 Introduction

The microstructurally small cracks are often initialized from persistent slip bands, at peaks of surface roughness or inhomogeneities in material. These cracks initially propagate on the slip planes and their crack propagation rates and paths are strongly influenced by local microstructural features. It has been found that grain boundaries, crystallographic orientations, inclusions, voids and material phases, etc. [1–3] affect the behaviour of such cracks. Grain boundary acts as microstructural obstacle and can result in a decrease of fatigue crack growth rate [3–5], crack arrest [6] or change the slip plane after the crack has passed the boundary [7]. The latter often results in zigzag patterns [8]. Different crystallographic orientations of the grains may also increase, decrease or arrest the crack growth [9,10]. The crack tip loading is therefore generally mixed-mode with strong shear component. The plastic zone size for these cracks is comparable to the crack length even at relatively small loads, therefore severely thwarting the applicability of linear elastic fracture mechanics.

To further our knowledge of these cracks further experimental work and modeling should be performed. Models should combine local microstructural features such as grain shapes, crystallographic orientations, etc. with advanced material models suitable for this length scale. A model for fatigue crack growth rate that includes the retardation of crack growth rate due to the grain boundary has been proposed in [11,12]. A combination of crystal plasticity and simplified grain modeling has been applied in [9,13–15] to study crack tip displacements, crack closure and crack tip plasticity and crack opening stresses. The authors concluded that both crack tip opening and sliding displacements contribute to

the crack growth [9], that plasticity induced crack closure will occur when the crack tip plastic zone is smaller than the grain size [16] and that the plastic zone size significantly depends upon the crystallographic orientation [13]. It was shown in [15] that the crack growth rate depends on the orientation of the adjacent grain. Crack growth rate in a single crystal was simulated in [14]. In these references grain shapes are not modeled explicitly. In recent years attempts have been made to account also for random grain shapes by either transfer of measured geometry to the model [17] or using Voronoi tessellation for modeling grain shapes [7,18]. Random grain geometry and crystal plasticity have been used in [19] where the scatter of the $J$-integral values for intergranular cracks has been determined

The present study builds on a previous work by authors [20], where the crack was confined to one surface grain only. Crystal plasticity is combined with random grain structure to investigate the effects of crystallographic orientations on a small transgranular, kinked crack embedded in a surface grain and extended across the grain boundary. Crack tip opening (CTOD) and sliding (CTSD) displacements are calculated for a stationary crack while the model is under monotonic uniaxial tensile load. Different crystallographic orientations are applied to provide: a) the dependence of crack tip displacements on the crystallographic orientation of a large grain 'wrapped' around the first (crack-containing) grain and b) the scatter of CTOD values due to the randomness of the grain structure.

The outline of the paper is as follows. The crystal plasticity is first presented. Next, a description of the finite element model with respect to kinematic constraints, boundary conditions and meshing is given. Finally, results for different crystallographic orientations and crack lengths are presented.

## 2 Model Description

### *2.1 Constitutive model*

Generalized Hooke's law is used for monocrystal's elastic behaviour, $\sigma_{ij} = C_{ijkl}\epsilon^e_{kl}$, where $\sigma_{ij}$ represents the second-rank elastic stress tensor, $C_{ijkl}$ the fourth-rank stiffness tensor and $\epsilon^e_{kl}$ the second-rank elastic strain tensor. The number of independent elastic constants for a cubic crystal system (BCC and FCC) is 3.

Crystal plasticity theory is used [21] to describe the material's plastic behaviour at the grain level. The plastic deformation in monocrystals is assumed to take place via a simple shear on a specific set of slip planes, see Fig. 1. Deformation by other mechanisms such as for example diffusion, twinning and grain boundary sliding is currently not taken into account. The combination of a slip plane, denoted by its normal $m^\alpha_i$, and a slip direction, $s^\alpha_i$, is called a slip system, $(\alpha)$. The plastic velocity gradient, $\dot{u}^p_{i,j}$, due to a crystallographic slip can be written as,

$$\dot{u}^p_{i,j} = \sum_\alpha \dot{\gamma}^{(\alpha)} s^{(\alpha)}_i m^{(\alpha)}_j, \tag{1}$$

where the summation is performed over all active slip systems, $(\alpha)$, while $\dot{\gamma}^{(\alpha)}$ represents the shear rate. The cumulative slip,$\gamma$, is defined as,

$$\gamma = \sum_\alpha \int_0^t \left|\dot{\gamma}^{(\alpha)}\right| dt. \tag{2}$$

It is assumed that the shear rate $\dot{\gamma}^{(\alpha)}$ depends on the stress only via the Schmid resolved shear stress, eq. (3). The Schmid resolved shear stress for a given slip

system is given by eq. (4). Yielding is then assumed to take place when the Schmid resolved shear stress exceeds the critical shear stress $\tau_0$.

$$\dot{\gamma}^{(\alpha)} = \dot{a}^{(\alpha)} \left( \frac{\tau^{(\alpha)}}{g^{(\alpha)}} \right) \left| \frac{\tau^{(\alpha)}}{g^{(\alpha)}} \right|^{n-1} \tag{3}$$

$$\tau^{(\alpha)} = s_i^{(\alpha)} \sigma_{ij} m_j^{(\alpha)} \tag{4}$$

In eq. (3), $\dot{a}^{(\alpha)}$ represents the reference strain rate, $n$ the strain-rate-sensitivity parameter and $g^{(\alpha)}$ the current strain-hardened state of the crystal. In the limit, as $n$ approaches infinity, this power law approaches that of a rate-independent material. The current strain-hardened state $g^{(\alpha)}$ can be derived from,

$$\dot{g}^{(\alpha)} = \sum_{\beta} h_{\alpha\beta} \quad \dot{\gamma}^{(\beta)}, \tag{5}$$

where $h_{\alpha\beta}$ are the slip-hardening moduli defined by the adopted hardening law. In this work Peirce et al. hardening law is used [22], where self-hardening moduli $h_{\alpha\alpha}$ are defined by:

$$h_{\alpha\alpha} = h_0 \mathrm{sech}^2 \left( \frac{h_0 \gamma}{\tau_s - \tau_0} \right), \quad \mathrm{sech} = 1/\cosh . \tag{6}$$

Here $h_0$ stands for the initial hardening modulus, $\tau_0$ the yield stress (equal to the initial value of the current strength $g^{(\alpha)}(0)$) and $\tau_s$ a reference stress where large plastic flow initiates [23]. The latent-hardening moduli $h_{\alpha\beta}$ are given by,

$$h_{\alpha\beta} = q h_{\alpha\alpha}, \qquad (\alpha \neq \beta), \tag{7}$$

where $q$ is a hardening factor. This model was implemented as a user-subroutine into the finite element code ABAQUS.

Macroscopic stress $< \sigma_{ij} >$ and strain tensors $< \epsilon_{ij} >$ are estimated using volume averaging. For comparison with engineering stress and strain Mises equivalent stress and strain are used. Further details on its theory and implementation can be found in [23,24].

### *2.2 Layout of Structural Model*

The structural model is a planar rectangular aggregate with 212 randomly sized and shaped grains. The grain structure is a planar Voronoi tessellation generated using code VorTESS [25]. The finite element model of the grain structure with a crack is presented in Fig. 2.

Each grain is subdivided into 8-noded, reduced-integration, plane strain finite elements. The finite element meshing of the grains away from the crack tip is automatic and follows procedures outlined in [26]. Only tessellations with reasonably small aspect ratios of cord lengths are considered as "meshable" with finite element software. Such approach essentially prevents use of tessellations with very small grains. Further details are available in [26]. The finite element meshing of the crack tip neighbourhood is detailed in Section 2.2.3.

Each grain is assumed to behave as a randomly oriented monocrystal governed by the anisotropic elasticity and crystal plasticity models as described in the previous section. The number of grains included in the model is not sufficient to result in a size-independent macroscopic response of the aggregate (Representative Volume Element). However, the experience with similar simulations shows that the error caused by this omission is limited to about 5 % [24].

The average grain size of 52.9 $\mu$m is used in the analysis. This agrees well with

values published for 316L steel being between 50 $\mu$m and 80 $\mu$m.

### *2.2.1 Crystallographic orientations*

Appropriate crystallographic orientations are achieved in two steps:

(1) In the first step the angle between the crystallographic [100] direction and the macroscopic X axis of all crystals in the model is set to 135 ° as shown in Fig. 1. This results in a planar slip system model compatible with the planar macroscopic model. The resulting projections of the primary and conjugate slip planes are illustrated in Fig. 3.

(2) In the second step, random orientation of grains is achieved by randomly rotating crystals around the global Z-axis. Uniform distribution with range 0 to $2\pi$ is used. Within the grain the initial crystallographic orientations are identical.

Application of the macroscopic tension in the X-direction results in macroscopic maximum shear stress planes at $\pm 45\,^{\circ}$ to the X-axis. Now, coincidence of macroscopic shear planes and microscopic primary and conjugate slip planes is achieved when the crystals are rotated around the Z axis for: $\alpha$ =9.735 °, 80.265 °, 99.735 ° or 170.265 ° as illustrated in Figure 3.

### *2.2.2 Loading and boundary conditions*

The applied macroscopic loading and boundary conditions are illustrated in Fig. 2. The left and right edges are loaded in macroscopic monotonic uniaxial tension up to a maximum load of $0.96 R_{p0.2}$ (240 MPa) with zero shear traction. This load is sufficient to trigger slip systems activity in all cases analyzed. The

upper and lower edges are traction free. Prevention of rigid body movement is also imposed.

### *2.2.3 The crack and the crack tip mesh*

A short inclined surface crack is introduced in the model with crack orientation in grain 38 fixed to 315 ° and different crack extension deflections in grain 124 (second grain), see Fig. 4.

Since it is our intention to model a Stage I fatigue crack, the grain crystallographic orientation is rotated so that the crack falls into either slip plane P2 or slip plane P4. The rather large complexity of including both crack growth and cyclic loading into the model is however avoided at this point in time and may be included in the model in the future. All results in this paper are therefore obtained assuming stationary crack and monotonic loading regime.

The CTOD and CTSD values are calculated at a distance of 2.5 % of the average grain size behind the crack tip (i.e. 0.025·52.9=1.3 $\mu$m), see Fig. 5. This is consistent with examples found in the literature [15,27].

Extensive mesh sensitivity study was performed, resulting in the optimal mesh shown in Fig. 2. The typical crack tip element size is about 0.125 $\mu$m. This is deemed sufficient for this analysis.

### *2.2.4 Material parameters*

The following elastic constants for AISI 316L single crystal are used: $C_{iiii}$= 163680 MPa, $C_{iijj}$= 110160 MPa, $C_{ijij}$= 100960 MPa [28]. Crystal plasticity parameters have been optimized from the macroscopic plastic response of AISI

316L polycrystal [28]. $h_0$= 330 MPa, $\tau_s$= 270 MPa, $\tau_0$= 90 MPa, $n$= 55, $q$=1.0 and $\dot{a}^{(\alpha)}$=0.001. With these parameters the proposed plain strain model is deemed sufficient to provide a correct qualitative representation of the macroscopic response.

## 3 Results

The primary goal in this paper is to assess the influence the random grain structure imposes on the CTOD of a kinked short crack. Investigation is focused on the randomness of orientations while keeping the grain shapes constant. This approach is expected to reveal most of the variability contributed by the random grain structure [29]. Two main cases are analyzed:

(1) Bicrystal configuration: the goal is to provide the dependence of CTOD on the crystallographic orientation of a large grain 'wrapped' around the first (crack-containing) grain. Also, the orientations and slip planes with extreme CTOD values are revealed.
(2) Polycrystal configuration: the scatter of CTOD values due to the randomness of the grain structure is investigated.

The same basic finite element model shown in Fig. 2 is used for the bicrystal and polycrystal case.

### *3.1 Bicrystal*

The crystallographic orientations ($\alpha$) and are as follows:

- Grain 38: $\alpha_{38}$=9.735 ° → crack in grain 38 falls into the slip plane P2.

- All other grains have identical crystallographic orientations, labeled as $\alpha_{124}$. As the crack has to be in the slip plane, the crystallographic orientation can be set so that the crack falls either into the slip plane P2, eq. (8), or into the slip plane P4, eq. (9). Both cases are analyzed. Crack extension deflection $\Delta\theta_{124}$ is varied from -75.186 ° up to 104.814 °, see Fig. 6.

$$\alpha_{P2} = (315^\circ + \Delta\theta_{124}) - 180^\circ - 90^\circ - 35.264^\circ \tag{8}$$

$$\alpha_{P4} = (315^\circ + \Delta\theta_{124}) - 180^\circ - 90^\circ + 35.264^\circ \tag{9}$$

To align the slip planes P2 or P4 with the crack extension, the crystallographic orientation of the grain in which crack extension lies in, has to be rotated appropriately. By doing so we change stiffness of this grain. In plastic region this stiffness is firstly defined by Schmid factors, Fig. 7, and secondly by applied power law for calculating the shear rate, eq. (3). Due to the high exponent in eq. (3), directions with slightly smaller Schmid factors will exhibit significantly decreased shear rate. The combination of the two factors results in certain directions giving stiff response, while others have soft response. Fig. 8 shows resulting different stiffness for a large monocrystal. Shaded bar above the figure represents directions resulting in purely elastic ( ), stiff elasto-plastic ( ) with $0 \leq \epsilon_{11}^{plastic} < 0.1\,\%$ and soft elasto-plastic response ( ) with $\epsilon_{11}^{plastic} \geq 0.1\,\%$.

As expected, the maximal plastic deformations occur at maximal Schmid factors on individual slip planes. The elastic part is not negligible and when added to the plastic part results in higher overall strain at $\alpha$ =80.265 ° and 99.735 ° compared to the overall strain at $\alpha$ =9.735 ° and 170.265 °.

The effect of all these factors on the CTOD of a bicrystal is presented in Fig. 9. Note that at each crack extension deflection angle, $\Delta\theta_{124}$, two cases having different crystallographic orientations are analyzed. One where the crack extension is in the slip plane P2 (solid line) and the other where it is in the slip plane P4 (dashed line). Two shaded bars on the top of the figure represent directions resulting in purely elastic ( ), stiff elasto-plastic ( ) and soft elasto-plastic response ( ). These two bars are taken from Fig. 8 and are shifted according to whether the crack extension falls into the slip plane P2 or P4. The corresponding crystallographic orientations are indicated next to the bars. These orientations are calculated using eq. (8) and eq. (9). Label $0.5D_{124}$ stands for the crack extension length being half the size of the grain 124, where $D_{124}$ stands for grain 124 size.

One can immediately observe that the highest CTODs (points A and C) are obtained at crystallographic orientations with soft elasto-plastic response, whereas the small CTODs are obtained when the response is purely elastic. The lowest CTOD are obtained when the crack extension deflects above $\Delta\theta_{124}$=38 ° and crack extension comes close to being parallel to external load. Low CTOD values are therefore expected. As the crack deflection increases above 45 ° CTOD values are additionally reduced due to a shift of the highest equivalent strains from the crack tip the point where the crack kinks. Similar effect was noticed for crack extension placed in slip plane P4.

If the crack extension deflection is 0 °, the crack does not kink. If additionally, the crack is placed in the slip plane P2 (point D), the crystallographic orientations are identical for both grains and we have a monocrystal configuration. Note that CTOD in this case ($\Delta\theta_{124}$=0 °) is actually smaller than when the crack is placed in the P4 slip plane (dashed line). The reason for

this is in the orientation of the crystal containing crack extension. To place the crack extension into the P4, the crystal is rotated at 80.264 ° which results in a softer response compared to 9.736 ° which is needed to place the crack into the slip plane P2, see Fig. 8. Since the maximal Schmid factors are the same for both angles of rotation, the main contributing factor resulting in this CTOD difference is caused by anisotropic elasticity.

A difference of 18 % in maximal CTOD values, see Fig. 9, is attributed to the difference in crack extension direction and slip plane. Maximal CTOD for crack extension in plane P4 is attained at crack extension deflection of -18 ° compared to 2 ° for placing the crack extension into the plane P2. Since at crack extension deflection of -18 ° the crack is closer to being perpendicular to external load, this configuration results in larger CTOD. A difference of 24 % in CTOD between the two crack extension directions was obtained using only isotropic elastic material model.

In addition to CTOD values Fig. 10 a) also shows CTSD values. It is evident that crystallographic orientations with soft elasto-plastic response also result in high CTSD values, while orientations resulting in pure elastic response decrease CTSD values. For the most of the configurations the CTOD and CTSD are only slightly shifted, which implies mixed-mode crack, see Fig. 10 b). The mode-mixity parameter, $\psi$, is here based on small scale yielding definition, eq. (10). $\psi = 0$ corresponds to pure Mode I whereas $\psi = 90\,^\circ$ corresponds to pure Mode II. The crack extensions deflections for which maximum CTOD are obtained are clearly mixed mode.

$$\psi = \arctan\left[\sqrt{\frac{CTSD}{CTOD}}\right] \tag{10}$$

The conclusions made so far are also valid for smaller external load of $0.8R_{p0.2}$, Fig. 11. One can see that a small reduction in load resulted in almost 4 times smaller CTOD values. Maximal CTODs are again obtained at crystallographic orientations resulting in soft elasto-plastic response. However, due to smaller amount of activated slip, areas of high CTODs are narrower compared to larger load, Fig. 9. Also, the relative difference between the peaks is now larger due to the increased elastic contribution to the overall deformation.

Analysis with shorter crack extension lengths at higher external load ($0.96R_{p0.2}$) was also performed, Fig. 12. It supports the conclusions obtained for the higher load-maximal CTOD values are obtained for configurations resulting in soft elasto-plastic response.

### *3.1.1 Preferential slip plane*

From a materials point of view it is more natural to present the computed crack opening displacements as function of the crystallographic orientation of the grain 124 rather than the kink angle. For a given crystallographic orientation Stage I crack propagation will take place in one of the slip planes (P2 or P4) as illustrated in Fig. 13. In Fig. 14 the CTOD is plotted versus the crystallographic orientation of grain 124 for the same load and crack length as in Fig. 9. We see that the computed CTOD vary significantly with grain orientation and that the maximum value for P2 (P4) is attained at $\alpha_{124}$=-8.264 $^\circ$ ($\alpha_{124}$=82.264 $^\circ$) with the associated kink angle $\Delta\theta_{124}$=-18 $^\circ$ ($\Delta\theta_{124}$=2 $^\circ$).

In the analysis it is assumed that the crack is in grain 124 once it crosses the grain boundary. As seen in Fig. 13 when the crystallographic orientation, $\alpha_{124}$, attains 114.550 $^\circ$ (5.079 $^\circ$) the slip plane P2 (P4) coincides with the grain

boundary. Because the crack is prescribed to remain in grain 124, the kink angle for P2 (P4) is changed in the analysis by 180° at this point. This is indicated with short dashed lines in Fig. 14. Due to the sudden jump in the kink angle, a jump in the CTOD is also observed in Fig. 14. It is to be noted that the meshing failed in some cases when a crack extension is very close to the grain boundary and for these cases the CTOD could not be computed. This is indicated with dotted lines in Fig. 14.

It is a logical assumption that the crack with a given crystallographic orientation will select the slip plane where the crack tip opening displacement is highest. In this case we can see that the difference in CTOD values due to different crystallographic orientation can be up to a factor of 7.7 (compare points B and C). It would also imply that the crack would propagate in plane P4 for 13.7°$\leq \alpha_{124} \leq$114.550° and in P2 for other grain orientations. There would also be a jump in the crack extension deflection angle as the preferential slip is changed from P2 to P4 (or vice versa), see Fig. 15. From such an argument it can also be inferred that the crack extension deflection angle will always be -75.141°$\leq \Delta\theta_{124} \leq$34°, Fig. 15. We saw in Fig. 10 that the crack tip loading is generally mixed mode. Thus the criterion for selecting the slip plane in which the crack would propagate should then be based on a more complex mixed mode criterion. However, since the CTOD and CTSD are more in less in phase, a mixed mode criterion would give approximately the same predicted kink angles.

We have seen that in this (bicrystal) case the influence of the crystallographic orientation of the grain surrounding the first cracked grain on the CTOD is quite large and more important than the crack extension direction. The difference in the CTOD for the points A and B in Fig. 14 is actually a factor

of 6.1. Even if the crack extension for point B is almost vertical, which should increase the CTOD, it is at its local minimum due to high stiffness of the large surrounding grain. Since in the polycrystal configuration the size of the second grain is much smaller, we expect that its stiffness will influence the CTOD less.

### *3.2 Polycrystal*

In this section 6 sets of polycrystal configurations are analyzed. Crystallographic orientation for the first two grains containing the crack (grains 38 and 124) are taken from orientations corresponding to points A, B, E, F, G and H of the bicrystal case in Fig. 14. Crystallographic orientation of the grain 38 is therefore always $\theta_{38}$=9.736 °. Corresponding orientations of the grain 124 are listed in Fig. 16. All remaining grains assume random crystallographic orientation. All together 100 different random subsets were generated for each of the 6 defined sets. Scatter due to the random nature of the crystallographic orientations is then calculated for two different crack extension lengths. The crystallographic orientations of the first two crack-containing grains and two used crack extension lengths are presented in Fig. 17 for the sets A and B.

Fig. 16 presents the cumulative probability functions. Small signs are related to smaller crack extension length. We can see that the influence of random crystallographic orientations in this case changes the CTOD by a factor of 3.3 for stiff grain 124 (purely elastic response, small '$_\circ$' signs) and by a factor of 3.1 for a soft grain 124 (soft elasto-plastic response, small '$_+$' signs). It is interesting that at this, shorter crack extension length a change in the crack extension direction only slightly changes the CTODs. A possible reason could

be that the influence of the first grain is still relatively large.

Another interesting property is that for both crack extension lengths the configuration with very stiff (purely elastic response) grain 124 results in higher CTODs, compare small and large '$_\circ$' and '$_+$' signs. In bicrystal case the situation was opposite since even if the stiffness of the second grain was the same, its size was so large that it almost surrounded the first one. This resulted in low CTOD values. In the polycrystal case, however, the secondary grain (grain 124) is only one of the neighbouring grains and one among many grains in the whole structure. Its relative influence is therefore decreased compared to the bicrystal case and consequently its stiffness has less impact on the CTODs.

While the influence of the stiffness of the second grain is decreased, the crack extension length and direction become much more important. We see from Fig. 16 that larger CTODs are obtained when the crack extension comes closer to being perpendicular to external load. The largest difference in the CTOD can be observed for $\times$ signs, with its maximal CTOD value approaching the largest CTOD value for the bicrystal case (point A in Fig. 14). Still, the difference between the maximal and minimal CTOD value, based on the 100 random subsets, is a factor of 3.3 which is similar to the shorter crack extension case. To determine the relation between the CTODs and crack extension direction, relation between these values is plotted in Fig. 18 for 10, 50 and 90 percentiles cases inferred from Fig. 16. A bicrystall relation is added for comparison, however it is highly unlikely that this configuration would occur and would correspond to a low probability tail of distribution. Fig. 18 confirms that the crack extension direction has a primary influence on the CTOD. The closer the crack extension is to being perpendicular to external load, the larger the CTODs are. The correlation is very good.

## 4 Conclusions

A study on the influence of the crystallographic orientations on the crack tip displacements of a microstructurally small crack, kinking while crossing the grain boundary, is presented. We presume that the crack growth is linked to the crack tip displacements. Although the loading in this paper is monotonic, a number of key observations are still relevant for the fatigue case.

For the bicrystal configuration the following conclusions can be made:

- The highest CTODs are obtained for crystallographic orientations with maximal Schmid factors on P2 and P4 planes. These orientations result in soft elasto-plastic response. On contrast, at small Schmid factors the response is purely elastic, resulting in small CTOD values. This suggests that the crack will preferably propagate through the soft grains compared to hard grains.
- Grain softness is defined by the crystallographic orientation. Anisotropic elasticity can be important as it can increase the grain stiffness at certain crystallographic orientations with maximal Schmid factors and decrease it for others. Crack will propagate on the slip plane defined with crystallographic orientation resulting in maximal Schmid factor and minimal stiffness coming from the elastic part. These two factors have to result in minimal overall grain stiffness for the CTOD to be maximized. At the macroscopic loads approaching the yield strength the anisotropic elasticity can still influence the CTODs by up to about 10 %.
- For a given crystallographic orientation there are always two possible slip planes. Assuming the crack follows the slip with the highest CTOD, the

crack would not deflect its direction bellow $\Delta\theta$=-75.141° and above $\Delta\theta$=34° while crossing the grain boundary.

- Crystallographic orientation of the grain surrounding the first crack-containing grain is more important than the crack extension direction.
- The crack tip loading is generally mixed mode.

For the polycrystal case the following conclusions can be made:

- Random orientations or grains beyond the first two crack-containing grains can change the CTOD by a factor of up to 3.3.
- The influence of the stiffness of the second crack-containing grain on the CTOD is significantly decreased as compared to the bicrystal case, while the crack extension direction becomes more important than the grain orientation.
- Largest CTOD values were obtained for slip planes that result in a crack extension being more perpendicular to the external uniaxial load. This suggest that among all the available slip planes the crack will most probably choose to propagate through the slip plane that is more perpendicular to the external load. This is in line with well known observation where small crack gradually transitions from Stage I to Stage II where its direction is perpendicular to the external load.

## References

[1] K. J. Miller, The behaviour of short fatigue cracks and their initiation. Part II-A general summary, Fatigue Fract. Engng. Mater. Struct. 10 (1987) 93–113.

[2] K. Hussain, Short fatigue crack behaviour and analytical models: a review,

Engng. Fract. Mech. 58 (1997) 327–354.

[3] K. Hussain, E. De los Rios, A. Navarro, A two-stage micromechanics model for short fatigue cracks, Engng. Fract. Mech. 44 (1993) 425–436.

[4] W. L. Morris, O. Buck, H. L. Marcus, Fatigue crack initiation and early propagation in Al 2219-T851, Metallurgical Transactions A. 7A (1976) 1161–1165.

[5] Y. H. Zhang, L. Edwards, On the blocking effect of grain boundaries on small crystallographic fatigue crack growth, Mater. Sci. Engng. A. 188 (1994) 121–132.

[6] S. Chakravarthula, Y. Qiao, Fatigue crack growth in a coarse-grained iron-silicon alloy, Int. J. Fatigue. 27 (2005) 1210–1214.

[7] O. Düber, B. Künkler, U. Krupp, H.-J. Christ, C.-P. Fritzen, Experimental characterization and two-dimensional simulation of short-crack propagation in an austenitic-ferritic duplex steel, Int. J. Fatigue. 28 (2006) 983–992.

[8] S. Suresh, Fatigue of materials, Cambridge University Press, 1991.

[9] V. Tvergaard, Y. Wei, J. W. Hutchinson, Edge cracks in plastically deforming surface grains, Eur. J. Mech. A Solids. 20 (2001) 731–738.

[10] T. Zhai, A. J. Wilkinson, J. W. Martin, A crystallographic mechanism for fatigue crack propagation through grain boundaries, Acta Mater. 48 (2000) 4917–4927.

[11] A. Navarro, E. De Los Rios, A microstructurally-short fatigue crack growth equation, Fatigue Fract. Engng. Mater. Struct. 11 (1988) 383–396.

[12] A. Ahmadi, H. Zenner, Simulation of microcrack growth for different load sequences and comparison with experimental results, Int. J. Fatigue. 27 (2005) 853–861.

[13] K. Gall, H. Sehitoglu, Y. Kadioglu, Plastic zones and fatigue-crack closure under plane-strain double slip, Metallurgical and materials transactions A. 27A (1996) 3491–3501.

[14] G. P. Potirniche, S. R. Daniewicz, J. C. Newman, Jr., Simulating small crack growth behaviour using crystal plasticity theory and finite element analysis, Fatigue Fract. Engng. Mater. Struct. 27 (2004) 59–71.

[15] G. P. Potirniche, S. R. Daniewicz, Analysis of crack tip plasticity for microstructurally small cracks using crystal plasticity theory, Engng. Fract. Mech. 70 (2003) 1623–1643.

[16] K. Gall, H. Sehitoglu, Y. Kadioglu, FEM study of fatigue crack closure under double slip, Acta Mater. 44 (1996) 3955–3965.

[17] E. Anagnostou, A. Brahme, C. Cornwell, B. El-Dasher, J. Fridy, M. F. Horstemeyer, A. R. Ingraffea, S.-B. Lee, A. Maniatty, R. Noack, J. Papazian, A. Rollett, D. Saylor, H. Weiland, Simulation of fatigue crack initiation and propagation in aluminum alloys using realistic microstructures, in: 11th International conference on fracture, March 20-25 2005, Turin, Italy, 2005.

[18] R. Lillbacka, E. Johnson, M. Ekh, A model for short crack propagation in polycrystalline materials, Engng. Fract. Mech. 73 (2006) 223–232.

[19] L. Cizelj, H. Riesch-Oppermann, Towards growth model for short intergranular cracks in elastoplastic polycrystalline aggregate, in: Proceedings Fontevraud 5 : International symposium Contribution of Materials Investigation to the Resolution of Problems Encountered in Pressurized Water reactors, Vol. 1, Fontevraud 5, 2002, 196–203.

[20] I. Simonovski, K.-F. Nilsson, L. Cizelj, Crack tip displacements of microstructurally small cracks in 316L steel and their dependance on

crystallographic orientations of grains, Fatigue Fract. Engng. Mater. Struct. (submitted for publication).

[21] R. Hill, J. R. Rice, Constitutive analysis of elastic-plastic crystals at arbitrary strain, J. Mech. Phys. Solids. 20 (1972) 401–413.

[22] D. Peirce, R. J. Asaro, A. Needleman, Material rate dependence and localized deformation in crystalline solids, Acta Metall. 31 (1983) 1951–1976.

[23] Y. Huang, A user-material subroutine incorporating single crystal plasticity in the ABAQUS finite element program, Tech. rep., Harvard University (1991).

[24] M. Kovač, L. Cizelj, Modeling elasto-plastic behavior of polycrystalline grain structure of steels at mesoscopic level, Nucl. Eng. Des. 235 (2005) 1939–1950.

[25] H. Riesch-Oppermann, Generation of 2–D random Poisson–Voronoi mosaics as framework for micromechanical modeling of polycrystalline materials-algorithm and subroutines description, Tech. Rep. FZKA 6325, Forschungszentrum Karlsruhe (1999).

[26] S. Weyer, A. Frohlich, H. Riesch-Oppermann, L. Cizelj, M. Kovač, Automatic finite element meshing of planar voronoi tessellations, Engng. Fract. Mech. 69 (2002) 945–958.

[27] V. P. Bennett, D. L. McDowell, Crack tip displacements of microstructurally small surface cracks in single phase ductile polycrystals, Engng. Fract. Mech. 70 (2003) 185–207.

[28] I. Simonovski, K.-F. Nilsson, L. Cizelj, Material properties calibration for 316L steel using polycrystalline model, in: 13th International Conference On Nuclear Engineering, May 16-20, 2005, Beijing, China, 2005.

[29] S. Weyer, Experimentelle untersuchung und mikromechanische modellierung des schädigungsverhaltens von aluminiumoxid unter druckbeanspruchung, Ph.D. thesis, Universität Karlsruhe (2001).

## Figures

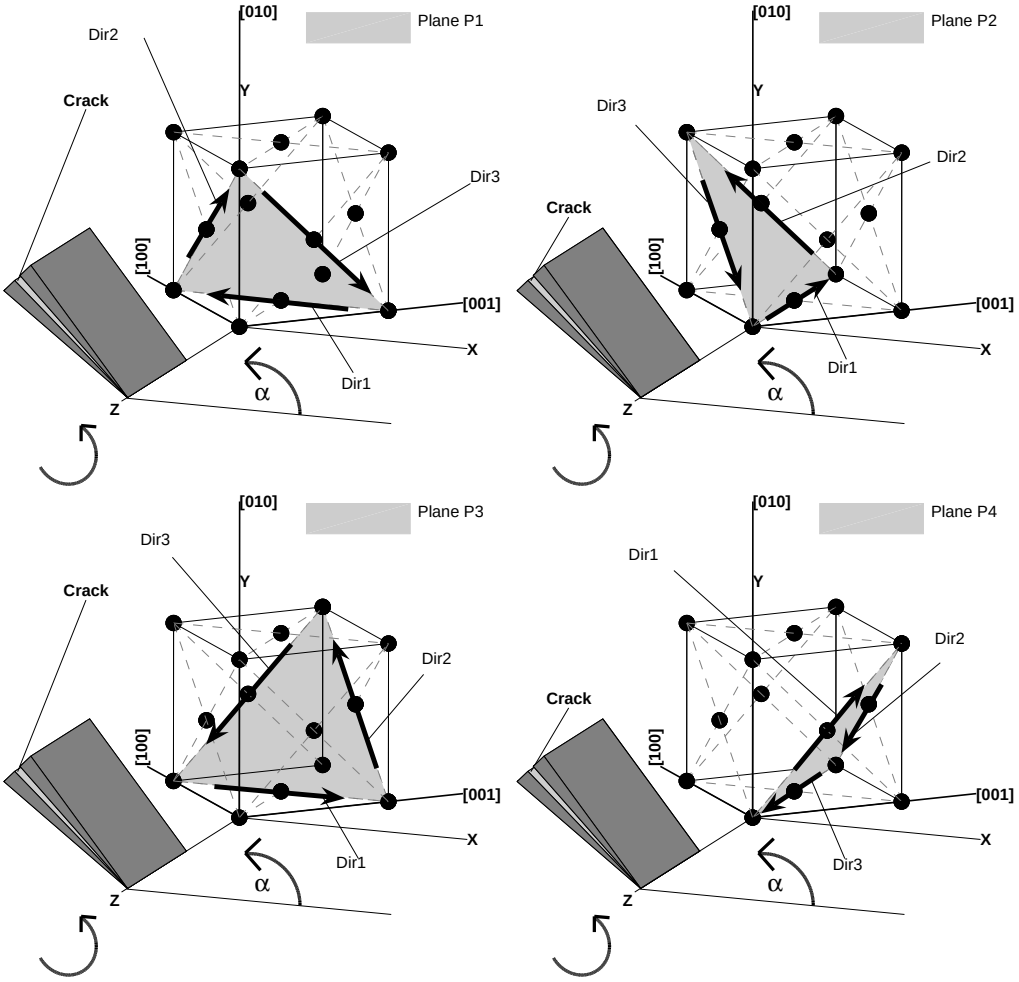


Fig. 1.

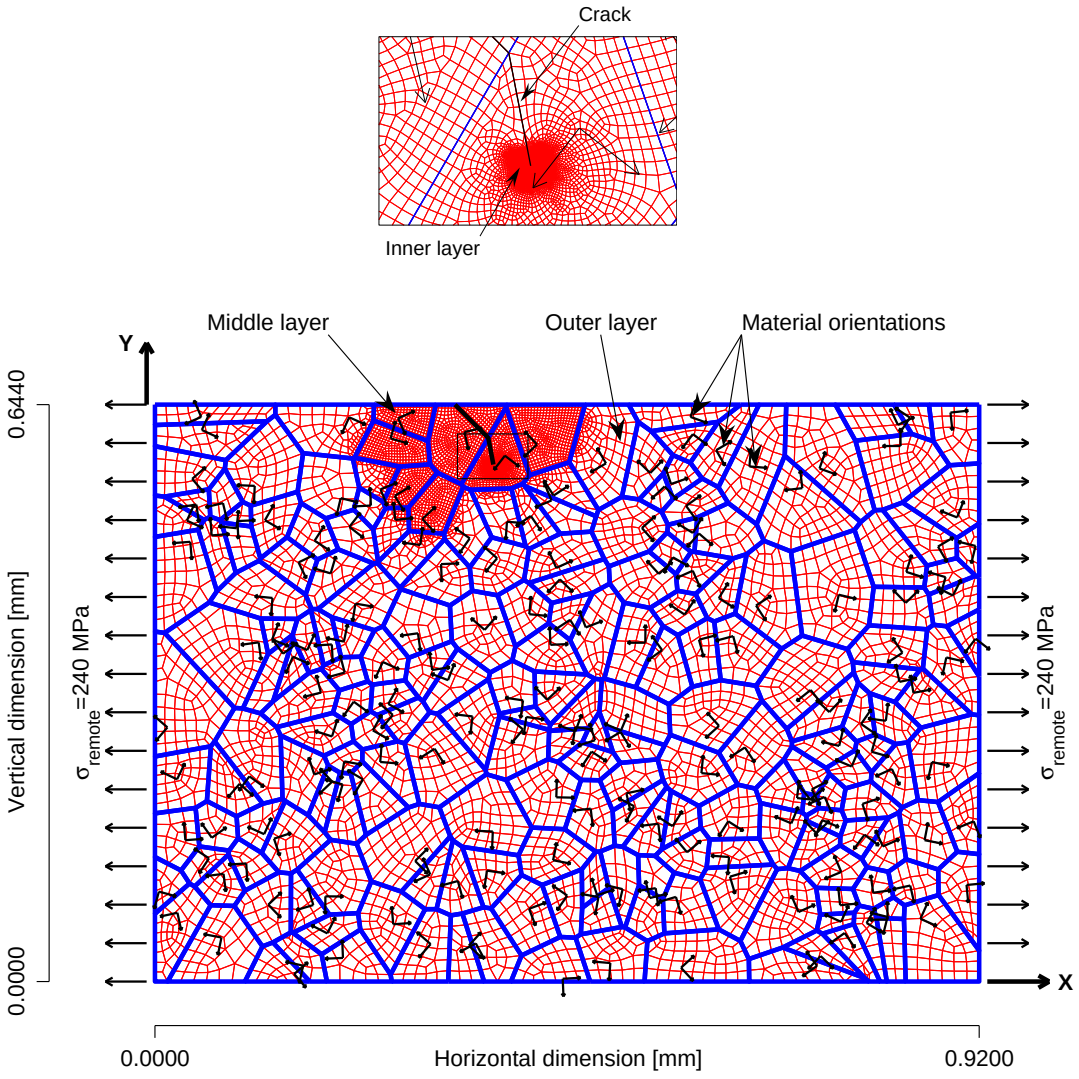
Crack
Inner layer
Middle layer
Outer layer
Material orientations
Y
X
0.6440
0.0000
Vertical dimension [mm]
σremote =240 MPa
σremote =240 MPa
0.0000
Horizontal dimension [mm]
0.9200

Fig. 2.

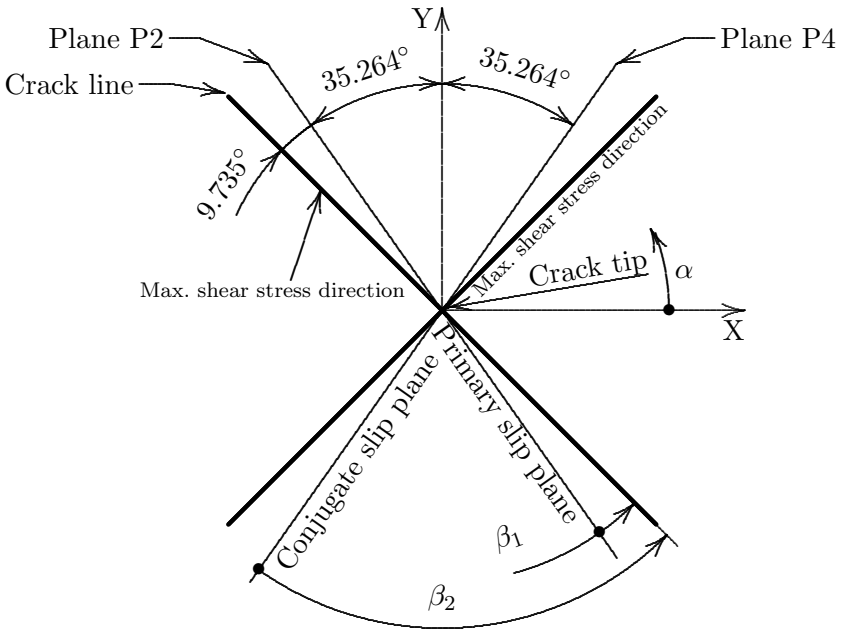


Fig. 3.

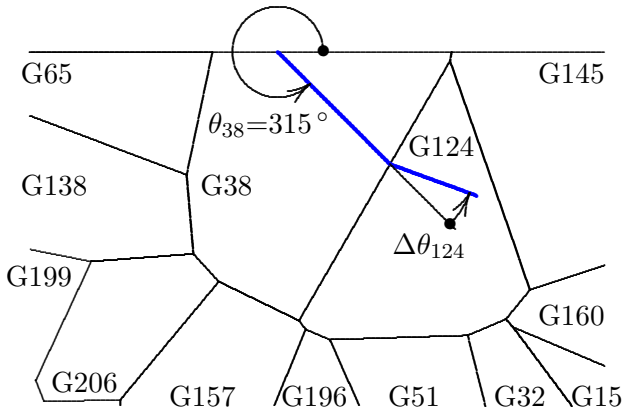


Fig. 4.

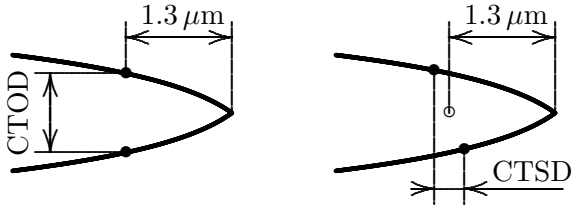


Fig. 5.

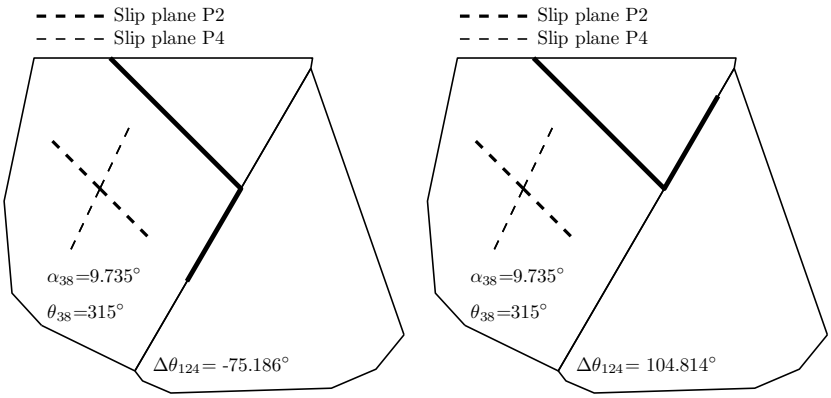
Slip plane P2
Slip plane P4
$\alpha_{38}$=9.735°
$\theta_{38}$=315°
$\Delta\theta_{124}$= -75.186°
Slip plane P2
Slip plane P4
$\alpha_{38}$=9.735°
$\theta_{38}$=315°
$\Delta\theta_{124}$= 104.814°

Fig. 6.

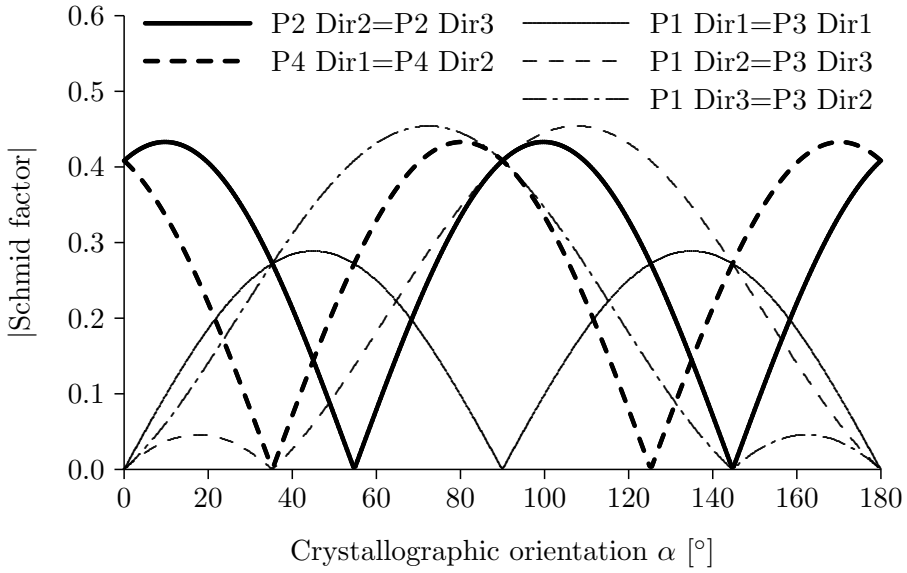
P2 Dir2=P2 Dir3
P4 Dir1=P4 Dir2
P1 Dir1=P3 Dir1
P1 Dir2=P3 Dir3
P1 Dir3=P3 Dir2
|Schmid factor|
0.0
0.1
0.2
0.3
0.4
0.5
0.6
0
20
40
60
80
100
120
140
160
180
Crystallographic orientation $\alpha$ [°]

Fig. 7.

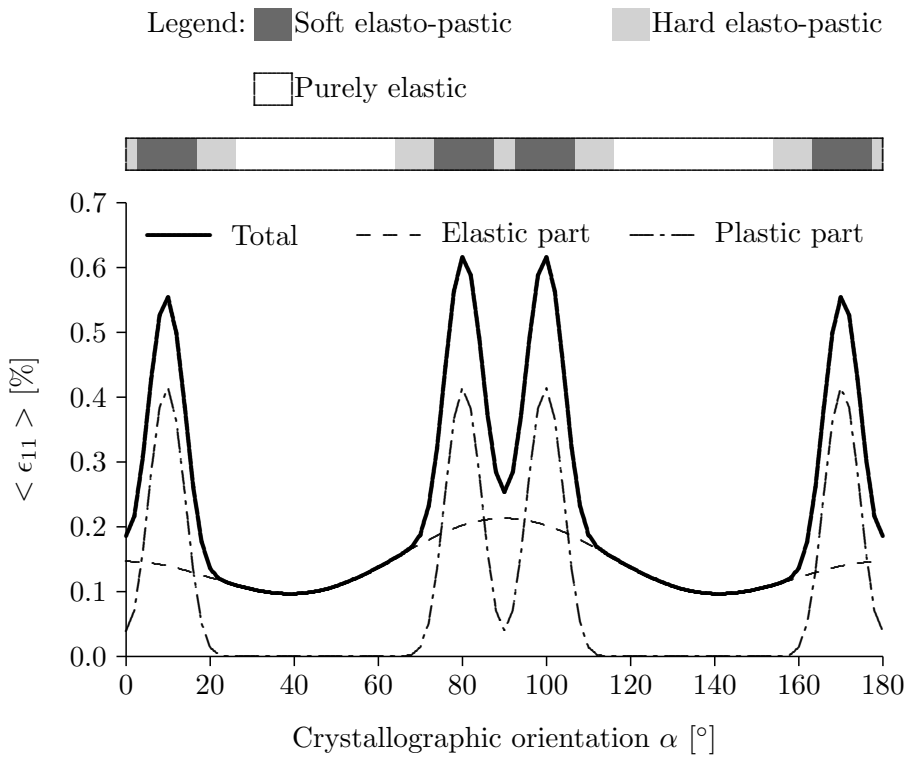
Legend:
Soft elasto-pastic
Hard elasto-pastic
Purely elastic
Total
Elastic part
Plastic part
< ϵ11 > [%]
0.0
0.1
0.2
0.3
0.4
0.5
0.6
0.7
0
20
40
60
80
100
120
140
160
180
Crystallographic orientation α [°]

Fig. 8.

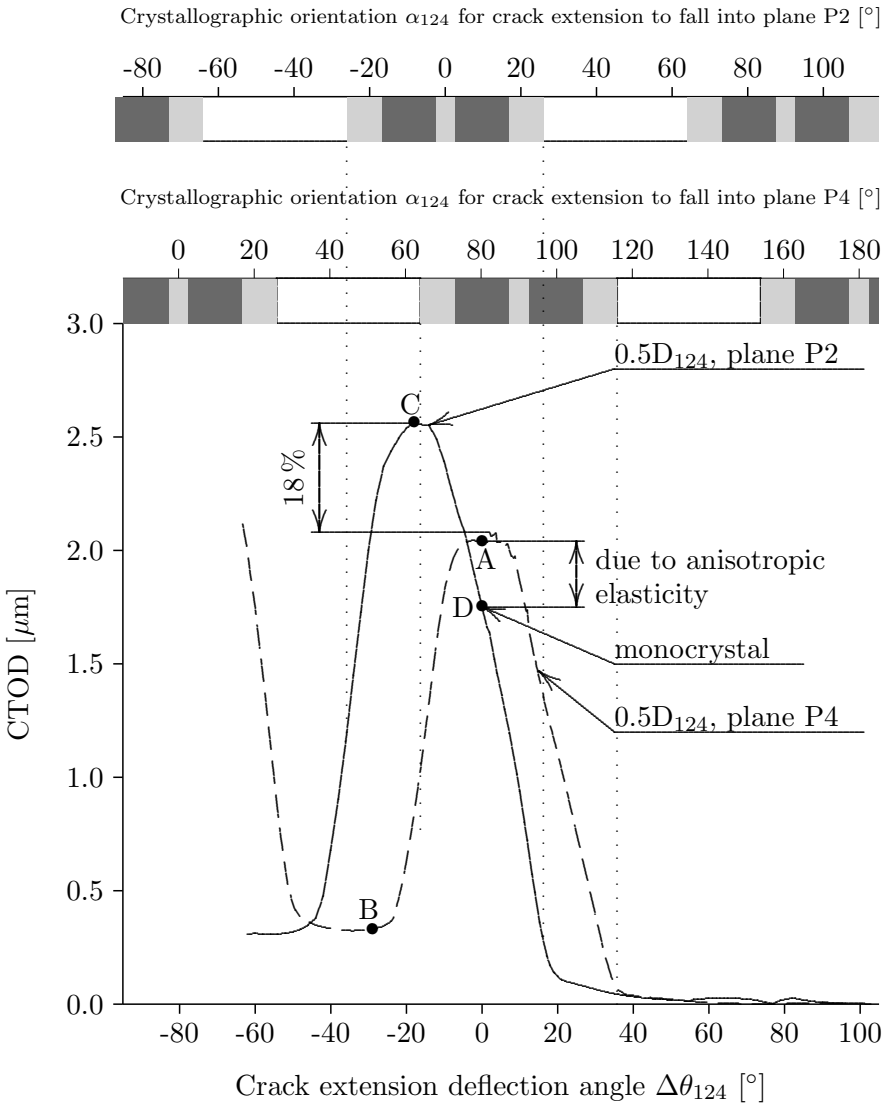
Crystallographic orientation $\alpha_{124}$ for crack extension to fall into plane P2 [°]
-80 -60 -40 -20 0 20 40 60 80 100
Crystallographic orientation $\alpha_{124}$ for crack extension to fall into plane P4 [°]
0 20 40 60 80 100 120 140 160 180
3.0
2.5
2.0
1.5
1.0
0.5
0.0
CTOD [$\mu$m]
$0.5D_{124}$, plane P2
C
18 %
A
due to anisotropic
elasticity
D
monocrystal
$0.5D_{124}$, plane P4
B
-80 -60 -40 -20 0 20 40 60 80 100
Crack extension deflection angle $\Delta\theta_{124}$ [°]

Fig. 9.

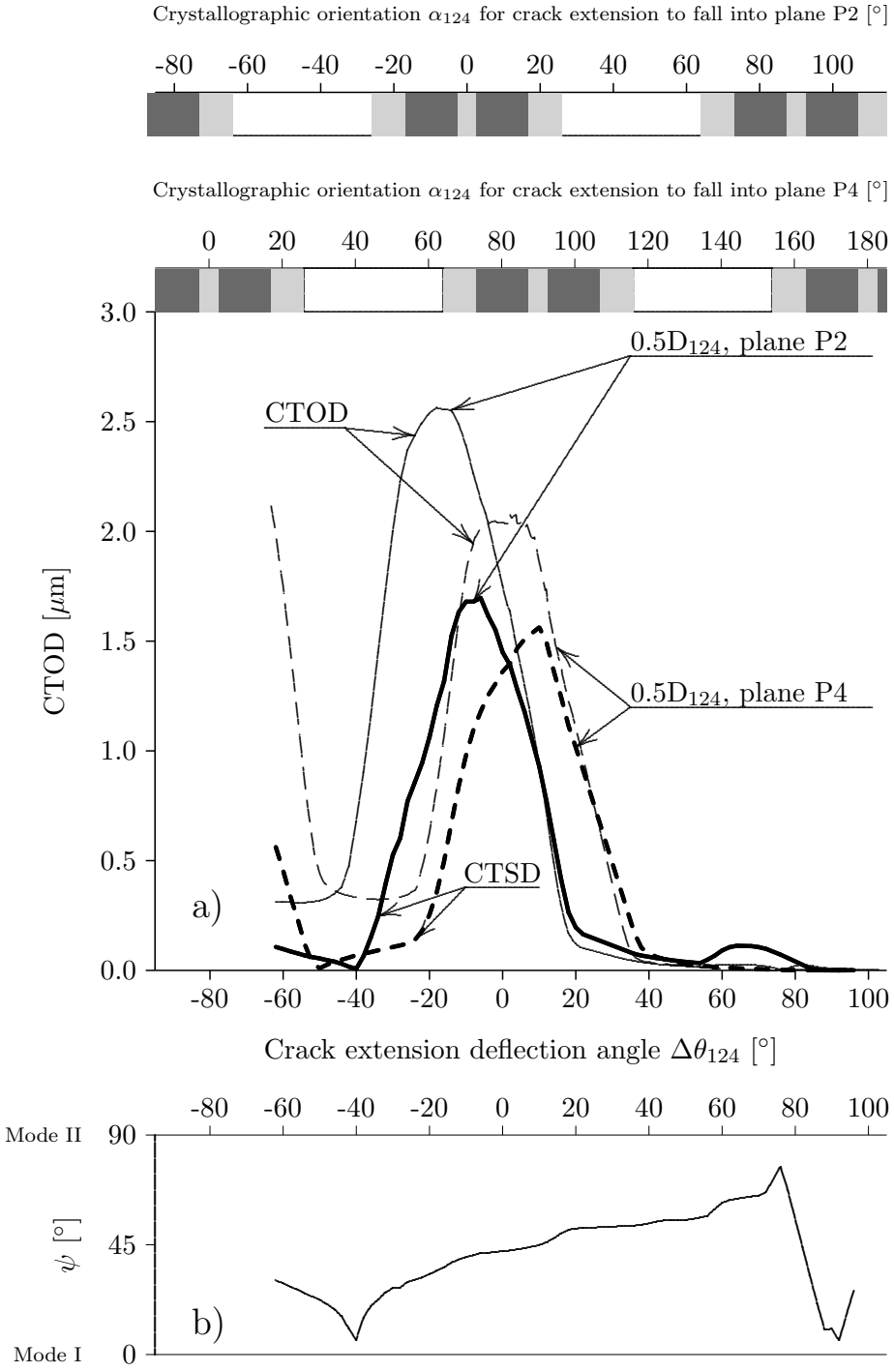
Crystallographic orientation $\alpha_{124}$ for crack extension to fall into plane P2 [°]
-80 -60 -40 -20 0 20 40 60 80 100
Crystallographic orientation $\alpha_{124}$ for crack extension to fall into plane P4 [°]
0 20 40 60 80 100 120 140 160 180
CTOD [$\mu$m]
3.0
2.5
2.0
1.5
1.0
0.5
0.0
0.5D$_{124}$, plane P2
CTOD
0.5D$_{124}$, plane P4
CTSD
a)
-80 -60 -40 -20 0 20 40 60 80 100
Crack extension deflection angle $\Delta\theta_{124}$ [°]
-80 -60 -40 -20 0 20 40 60 80 100
Mode II
90
$\psi$ [°]
45
b)
Mode I
0

Fig. 10.

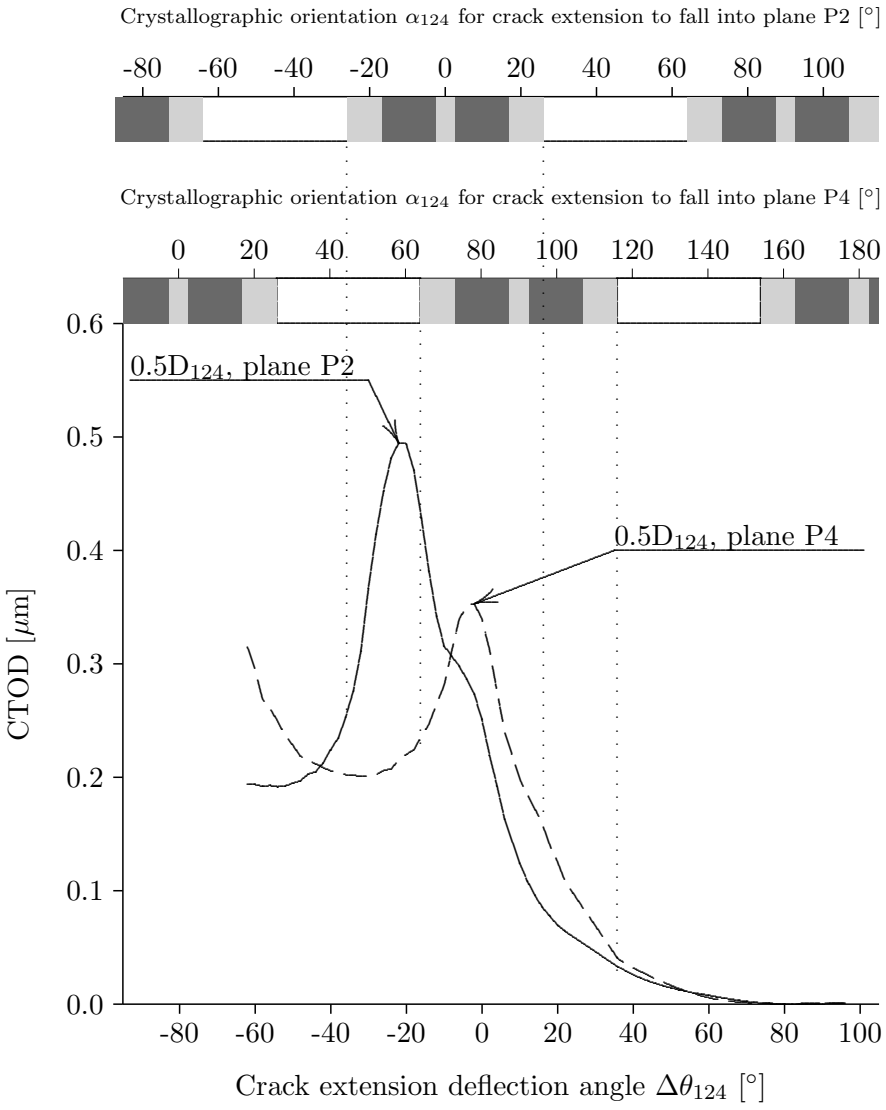
Crystallographic orientation $\alpha_{124}$ for crack extension to fall into plane P2 [°]
-80 -60 -40 -20 0 20 40 60 80 100
Crystallographic orientation $\alpha_{124}$ for crack extension to fall into plane P4 [°]
0 20 40 60 80 100 120 140 160 180
0.6
0.5
0.4
0.3
0.2
0.1
0.0
CTOD [$\mu$m]
$0.5D_{124}$, plane P2
$0.5D_{124}$, plane P4
-80 -60 -40 -20 0 20 40 60 80 100
Crack extension deflection angle $\Delta\theta_{124}$ [°]

Fig. 11.

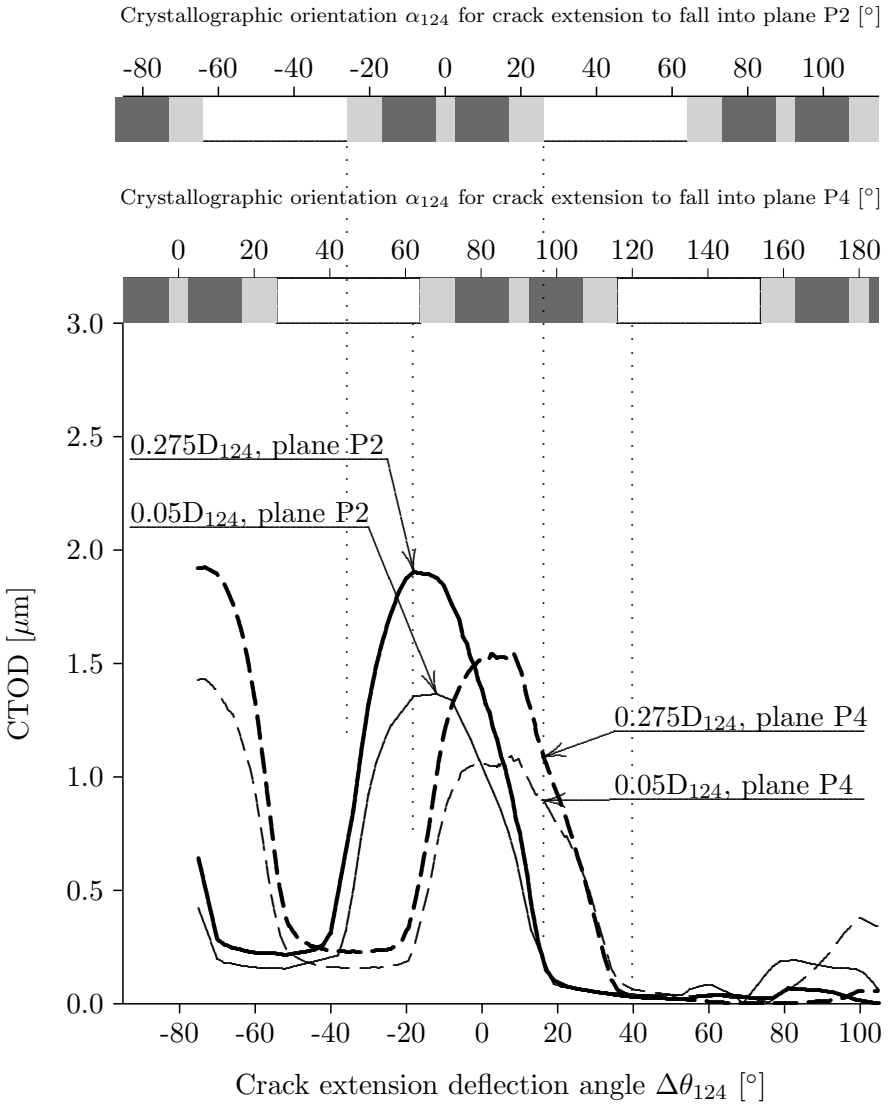
Crystallographic orientation $\alpha_{124}$ for crack extension to fall into plane P2 [°]
-80 -60 -40 -20 0 20 40 60 80 100
Crystallographic orientation $\alpha_{124}$ for crack extension to fall into plane P4 [°]
0 20 40 60 80 100 120 140 160 180
3.0
2.5
2.0
1.5
1.0
0.5
0.0
CTOD [$\mu$m]
0.275D$_{124}$, plane P2
0.05D$_{124}$, plane P2
0.275D$_{124}$, plane P4
0.05D$_{124}$, plane P4
-80 -60 -40 -20 0 20 40 60 80 100
Crack extension deflection angle $\Delta\theta_{124}$ [°]

Fig. 12.

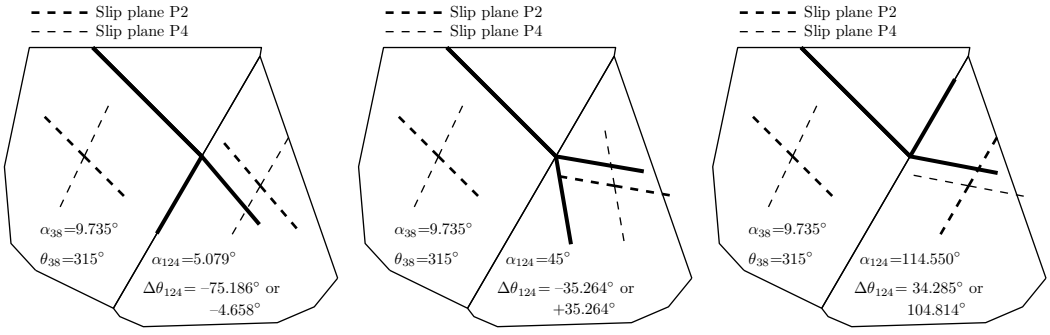
Slip plane P2
Slip plane P4
$\alpha_{38}$=9.735°
$\theta_{38}$=315°
$\alpha_{124}$=5.079°
$\Delta\theta_{124}$= –75.186° or –4.658°
Slip plane P2
Slip plane P4
$\alpha_{38}$=9.735°
$\theta_{38}$=315°
$\alpha_{124}$=45°
$\Delta\theta_{124}$= –35.264° or +35.264°
Slip plane P2
Slip plane P4
$\alpha_{38}$=9.735°
$\theta_{38}$=315°
$\alpha_{124}$=114.550°
$\Delta\theta_{124}$= 34.285° or 104.814°

Fig. 13.

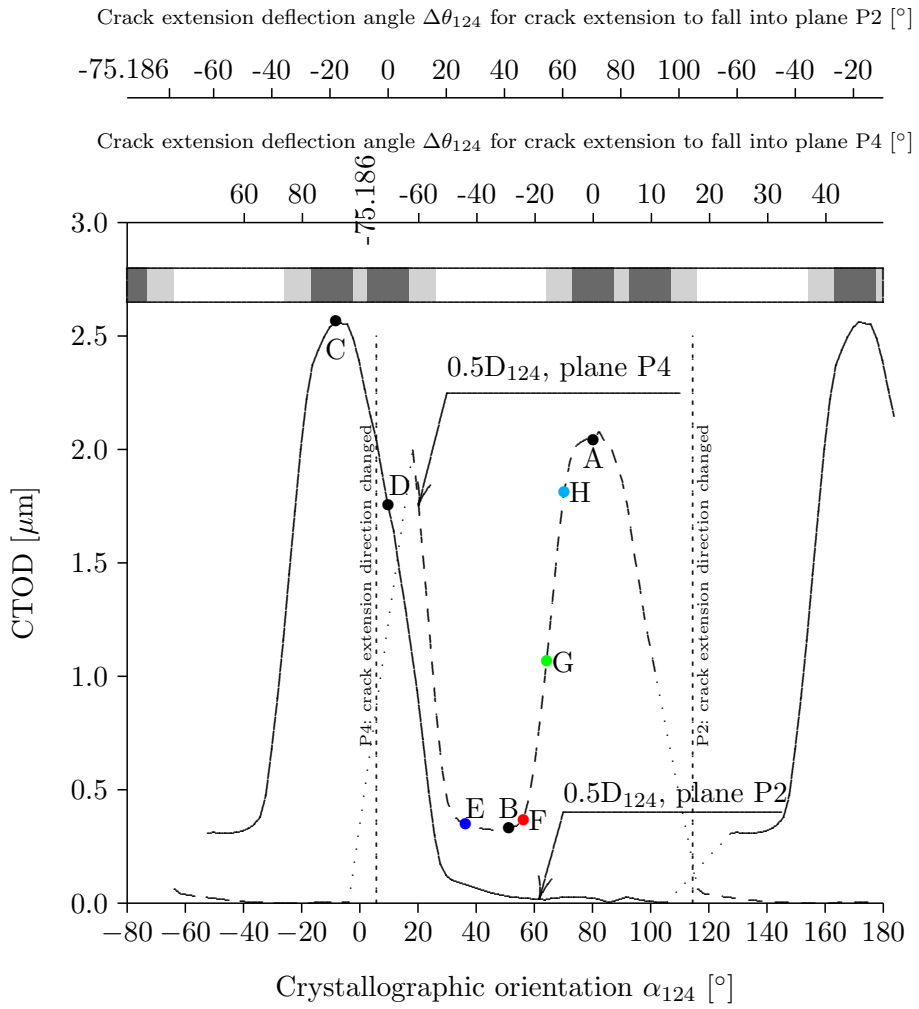
Crack extension deflection angle $\Delta\theta_{124}$ for crack extension to fall into plane P2 [°]
-75.186 -60 -40 -20 0 20 40 60 80 100 -60 -40 -20
Crack extension deflection angle $\Delta\theta_{124}$ for crack extension to fall into plane P4 [°]
60 80 -75.186 -60 -40 -20 0 10 20 30 40
3.0
2.5
2.0
1.5
1.0
0.5
0.0
CTOD [$\mu$m]
C
D
A
H
G
E
B
F
$0.5D_{124}$, plane P4
$0.5D_{124}$, plane P2
P4: crack extension direction changed
P2: crack extension direction changed
−80 −60 −40 −20 0 20 40 60 80 100 120 140 160 180
Crystallographic orientation $\alpha_{124}$ [°]

Fig. 14.

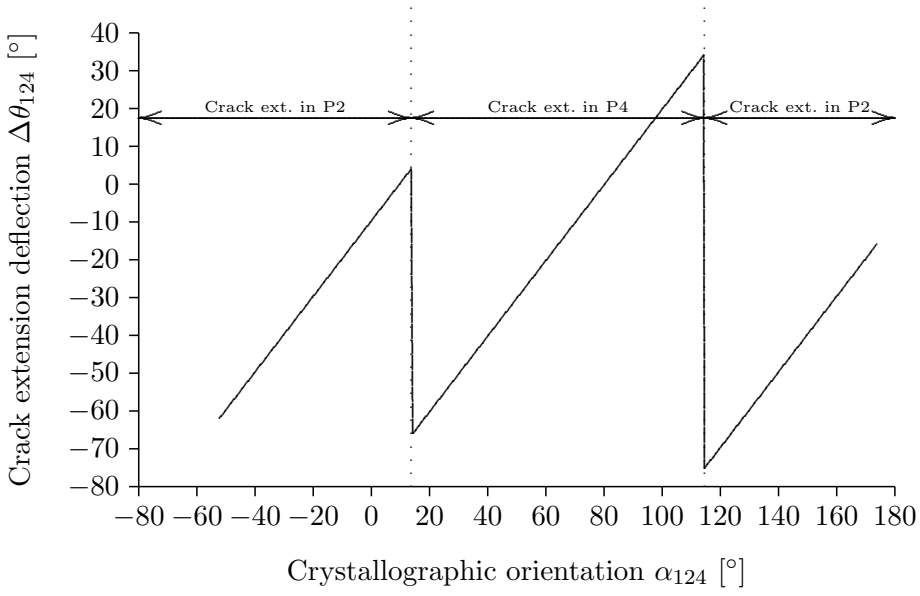
Crack extension deflection $\Delta\theta_{124}$ [°]
40
30
20
10
0
−10
−20
−30
−40
−50
−60
−70
−80
Crack ext. in P2
Crack ext. in P4
Crack ext. in P2
−80 −60 −40 −20 0 20 40 60 80 100 120 140 160 180
Crystallographic orientation $\alpha_{124}$ [°]

Fig. 15.

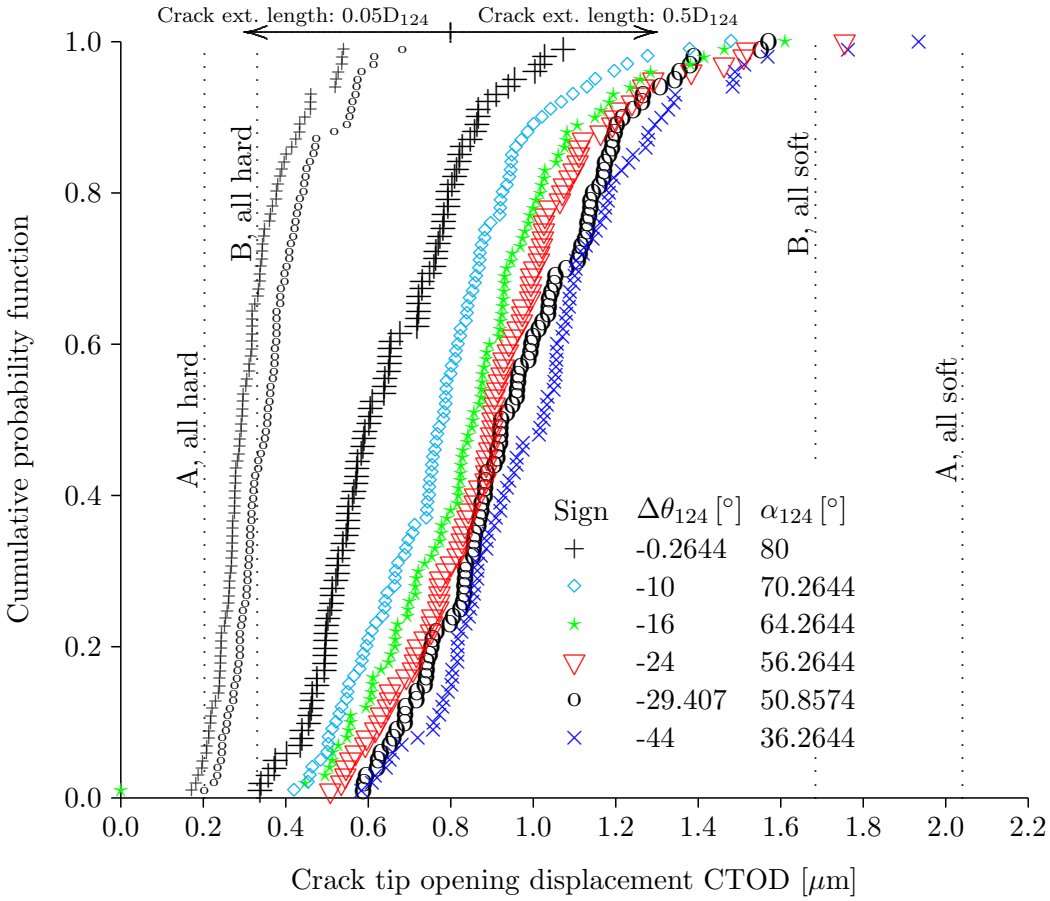
Crack ext. length: 0.05D124
Crack ext. length: 0.5D124
A, all hard
B, all hard
B, all soft
A, all soft
Cumulative probability function
Crack tip opening displacement CTOD [μm]
Sign
Δθ124 [°]
α124 [°]
+ -0.2644 80
◇ -10 70.2644
★ -16 64.2644
▽ -24 56.2644
o -29.407 50.8574
× -44 36.2644

Fig. 16.

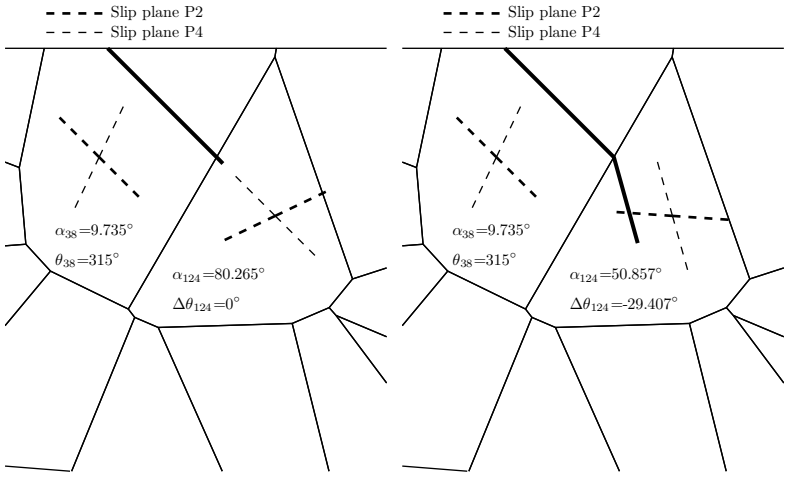
Slip plane P2
Slip plane P4
α38=9.735°
θ38=315°
α124=80.265°
Δθ124=0°
Slip plane P2
Slip plane P4
α38=9.735°
θ38=315°
α124=50.857°
Δθ124=-29.407°

Fig. 17.

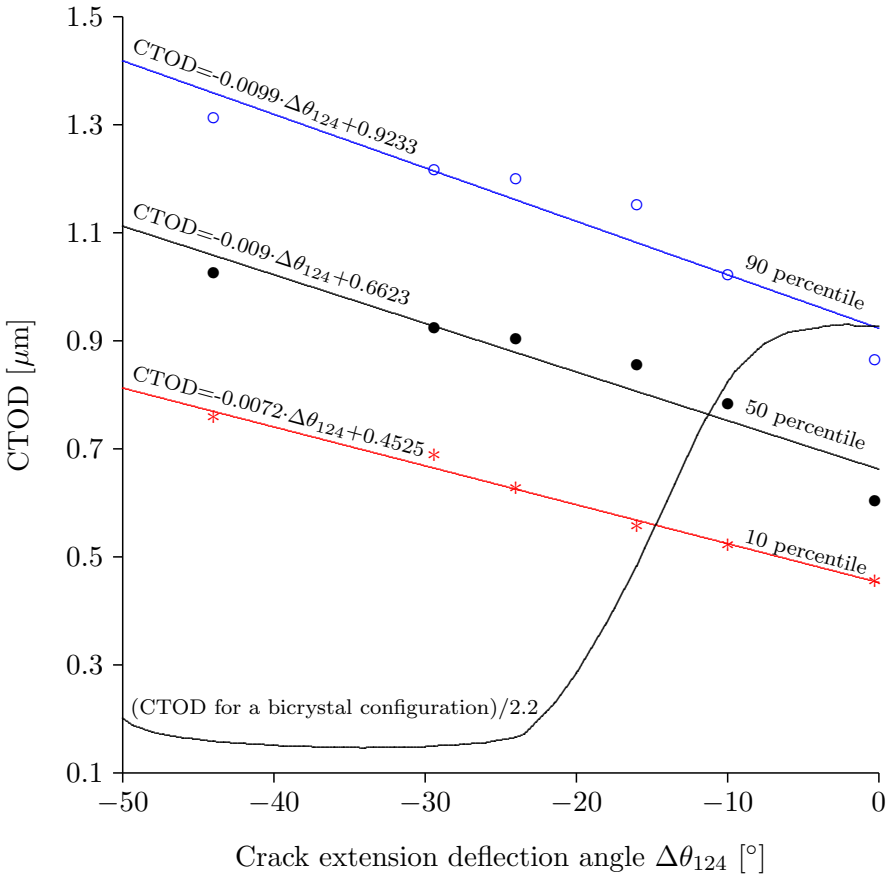
1.5
1.3
1.1
0.9
0.7
0.5
0.3
0.1
CTOD [μm]
CTOD=-0.0099·Δθ124+0.9233
CTOD=-0.009·Δθ124+0.6623
CTOD=-0.0072·Δθ124+0.4525
90 percentile
50 percentile
10 percentile
(CTOD for a bicrystal configuration)/2.2
−50
−40
−30
−20
−10
0
Crack extension deflection angle Δθ124 [°]

Fig. 18.

**List of Figures**

Fig. 10. Bicrystal: a) the influence of the crack extension deflection on the crack tip displacements and b) corresponding mode-mixity parameter $\psi$. Crack extension $0.5\mathrm{D}_{124}$, remote load $0.96R_{p0.2}$.

Fig. 11. Bicrystal: the influence of the crack extension deflection on the crack tip displacements for crack extension $0.5\mathrm{D}_{124}$. Remote load $0.8R_{p0.2}$.

Fig. 12. Bicrystal: the influence of the crack extension deflection the crack tip displacements for crack extensions $0.275\mathrm{D}_{124}$ and $0.05\mathrm{D}_{124}$. Remote load $0.96R_{p0.2}$.

Fig. 13. Different crack extension deflections, depending upon the slip plane that the extension falls in.

Fig. 14. Bicrystal: relation between the crystallographic orientation, grain hardness and crack extension deflection angle when the crack is placed in slip plane P2 or P4. Crack extension $0.5\mathrm{D}_{124}$, remote load $0.96R_{p0.2}$. Dotted lines indicate the lack of data due to mesh failure.

Fig. 15. Bicrystal: dependence of the crack deflection angle on the crystallographic orientation. Crack extension $0.5\mathrm{D}_{124}$, remote load $0.96R_{p0.2}$.

Fig. 16. CTOD histograms. Remote load $0.96R_{p0.2}$.

Fig. 17. Crystallographic orientations of the first two crack-containing grains for two used crack lengths and sets A and B. Orientations of all other grains are random.

Fig. 18. Relation between the crack extension deflection and CTOD for a polycrystal case. Remote load $0.96R_{p0.2}$, crack extension length $0.5\mathrm{D}_{124}$.